

Accelerating Visual Reinforcement Learning with Separate Primitive Policy for Peg-in-Hole Tasks

Zichun Xu¹, Zhaomin Wang¹, Yuntao Li¹, Lei Zhuang¹, Zhiyuan Zhao², Guocai Yang¹, and Jingdong Zhao^{1,*}

Abstract—For peg-in-hole tasks, humans rely on binocular visual perception to locate the peg above the hole surface and then proceed with insertion. This paper draws insights from this behavior to enable agents to learn efficient assembly strategies through visual reinforcement learning. Hence, we propose a Separate Primitive Policy (S2P) to simultaneously learn how to derive location and insertion actions. S2P is compatible with model-free reinforcement learning algorithms. Ten insertion tasks featuring different polygons are developed as benchmarks for evaluations. Simulation experiments show that S2P can boost the sample efficiency and success rate even with force constraints. Real-world experiments are also performed to verify the feasibility of S2P. Ablations are finally given to discuss the generalizability of S2P and some factors that affect its performance.

I. INTRODUCTION

Peg-in-hole is a popular assembly scenario but challenging, where slight misalignment can lead to failure. Narrow clearances and frequent contacts make traditional motion planning methods inefficient and increase unnecessary manual calibration costs. With its learning and robust adaptation capabilities, reinforcement learning (RL) can continuously refine the output action and adapt to changing conditions through trial and error. The usual modalities, such as vision [1], force/torque [2], and tactile [3], can be provided as observations to the agent to infer appropriate actions. Considering the hardware conditions, sensor noise, and the inability to obtain the pose information of holes in real scenarios, visual modality can be accessed at a lower cost and is a reasonable choice. Thus, visual reinforcement learning has been extensively explored in recent years, primarily involving generalization and sample efficiency [4], [5].

However, since the RL process relies heavily on extensive transitions, it raises higher demand on extracting valuable information from high-dimensional observations with fewer computational resources. Data augmentation [6] can effectively improve the sample efficiency of model-free RL algorithms. Moreover, policy design can be leveraged to further accelerate the insertion progress. Previous studies [7], [8] artificially defined different motion primitives and trained

This work is supported by the National Natural Science Foundation of China under the Basic Science Center Program for "Space Robot Intelligent Manipulation" under Grant No. T 2388101 and the National Natural Science Foundation of China (NSFC) under Grant No. 62403171.

¹State Key Laboratory of Robotics and Systems, Harbin Institute of Technology, Harbin 150001, Heilongjiang Province, China.

²School of Mechanical Engineering, Shandong University, Jinan 250061, China.

*Corresponding author: zhaojingdong@hit.edu.cn

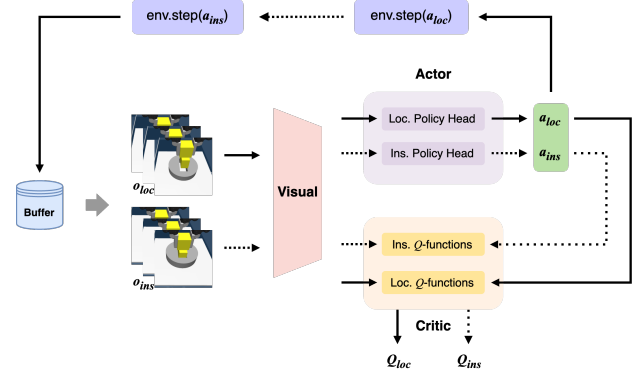


Fig. 1. Overview of the proposed insertion strategy. The encoded visual representations are passed to the actor to infer location and insertion actions, which will be performed sequentially. The output actions are fed to the critic with an ensemble of Q -functions to evaluate the corresponding Q -values.

policies to explore various combinations of them. However, designing and defining primitives are tedious and require extensive experiments. Analyzing the human insertion behavior, the entire sequence can be roughly interpreted as the mix of location and insertion. When insertion fails, subsequent adjustments are performed to relocate and reinsert, which will be repeated until success.

Inspired by the above, this paper presents a **Separate Primitive Policy (S2P)** to accelerate the visual RL progress. Two separate policies are trained simultaneously to derive location and insertion actions, respectively, which are executed sequentially by the agent. Ensemble Q -functions [9] are utilized to estimate Q -values for separate actions, and a higher update-to-data (UTD) [10] ratio is set to further enhance the sample efficiency. The proposed framework is adapted to model-free visual RL algorithms. Many insertion tasks, including different shapes of pegs and holes, are designed to verify the effectiveness of this strategy. Simulation results demonstrate that S2P can accelerate the insertion progress with higher success rates. The feasibility of S2P is also validated with the real-world experiment. The main contributions of this paper are as follows:

- 1) We propose a separate primitive policy based on the model-free visual reinforcement learning framework for peg-in-hole tasks.
- 2) The proposed method can effectively accelerate the sample efficiency and success rate even with strict force constraints.

- 3) A suite of peg-in-hole tasks integrated in simulation and the real-world experiment validate the effectiveness of our method.

II. RELATED WORK

Reinforcement Learning for Peg-in-Hole. RL can automate the repetitive insertion process and realize compliance through impedance control [11]. The target objects span from common primitives to industrial connectors, such as RJ45 in the NIST Task Board [12]. In recent years, different modalities have been fused to extract more features for complex insertion tasks with tight clearance [13], [14]. Tactile [3], [15] and force/torque [16] can sense more contact details and allow for higher pose uncertainty than that offered by vision. However, training and tuning in the real platform is impractical, and thus verification in simulation plays an important role. For the simulation results to be instructive, the discrepancies in the presentation of modality data and physical properties between simulation and reality must be considered. Additional methods are required to process the native signals obtained from the simulator to align the performance of real sensors [17]. The noisy nature of the force/torque signals means many transition states will not be experienced during training. In contrast, vision and robot proprioception are low-cost and easy to access [18]. Visual RL has been proven to be effective to accomplish insertion tasks [19], [20]. Even from the multimodal perspective, visual is an essential component, which is our intention to accelerate the visual RL process. [7] and [21] have utilized predefined primitives to replace low-level motion commands to reduce the task complexity and shorten the horizon. Nevertheless, both of them are performed with known state information of the hole, which is inconsistent with the reality. Thus, we design a visual-based insertion strategy and adopt only two primitives with location and insertion.

Visual Reinforcement Learning. Visual RL has shown great promise in dealing with complex manipulation tasks [22]. Due to the complex dynamics modeling of model-based algorithms, the majority of visual RL research has been conducted upon model-free algorithms. Improving sample efficiency and generalizability is fundamental in the visual RL domain [23], and data augmentation serves as a pivot to bridge these two areas. Image-level data augmentation intuitively improves the data efficiency by expanding the diversity of observation samples [24]. The agent can be endowed with better generalization capability during the training process. To further release the power of data enhancement, changes to the underlying algorithms are also necessary. The representative visual RL algorithm DrQ [25] and its successor DrQ-v2 [26] are compatible with data augmentation and can improve sample efficiency. Some additional recipes are employed to reduce the overestimation of Q-value and stabilize the training process [6], [27]. In addition, pre-trained visual encoders [1] and well-designed contrastive learning schemes [5], [28] can achieve competitive generalization performance. These visual encoders can be obtained by training on out-of-domain datasets but can

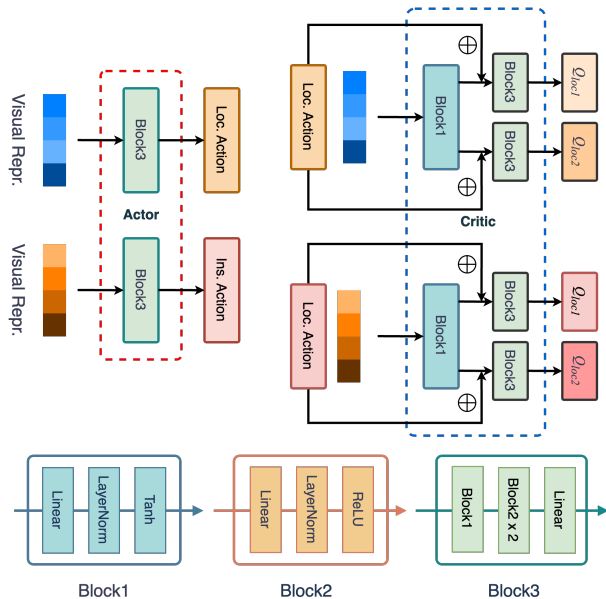


Fig. 2. Network architectures for the actor and critic of S2P-DrQ-v2.

improve the performance of agents on downstream tasks [29], [30]. These impressive results shed light on visual RL, but there are still challenges for making decisions in complex scenarios. Unlike the above studies, we focus on the insertion strategy design to accelerate the sample efficiency.

III. PRELIMINARIES

Visual RL can be formulated as an infinite-horizon Partially Observable Markov Decision Process (POMDP) [31] with the tuple $\langle \mathcal{O}, \mathcal{A}, \mathcal{P}, \mathcal{R}, \gamma \rangle$, where \mathcal{O} is the observation space with a stack of consecutive images $(\mathbf{o}_{t-k}, \dots, \mathbf{o}_{t-1}, \mathbf{o}_t)$, \mathcal{A} is the action space, $\mathcal{P}(\mathbf{o}_{t+1} | \mathbf{o}_t, \mathbf{a}_t)$ defines the transition function, $\mathcal{R} : \mathcal{O} \times \mathcal{A} \rightarrow \mathbb{R}$ denotes the reward function, and $\gamma \in [0, 1)$ is the discount factor. Starting from the initial state $\mathbf{o}_0 \in \mathcal{O}$, the objective is to learn an optimal policy π^* that maximizes the expected sum of discount rewards $\mathbb{E}_{\mathbf{a}_t \sim \pi(\cdot | \mathbf{s}_t), \mathbf{o}_t \sim \mathcal{P}} [\sum_{t=1}^{\infty} \gamma^t r_t]$.

IV. METHOD

A. Visual Reinforcement Learning Backbone

DrQ-v2 [26], an extension of DDPG [32], is an off-policy RL algorithm for visual continuous control. Clipped double Q-learning [33] and n -step returns are integrated into DrQ-v2 to reduce the overestimation bias and better estimate the temporal difference (TD) error, respectively. For each update, a batch of transitions $\tau = (\mathbf{o}_t, \mathbf{a}_t, r_{t:t+n-1}, \mathbf{o}_{t+n})$ is sampled from the replay buffer \mathcal{D} and then used to derive the critic loss:

$$\mathcal{L}_Q = \mathbb{E}_{\tau \sim \mathcal{D}} \left[(Q_{\phi_k}(\mathbf{h}_t, \mathbf{a}_t) - y)^2 \right] \quad \forall k \in \{1, 2\}, \quad (1)$$

where $\mathbf{h}_t = f_{\xi}(\text{aug}(\mathbf{o}_t))$, $\text{aug}(\cdot)$ is the customized data augmentation method, and f_{ξ} is the visual encoder. The n -

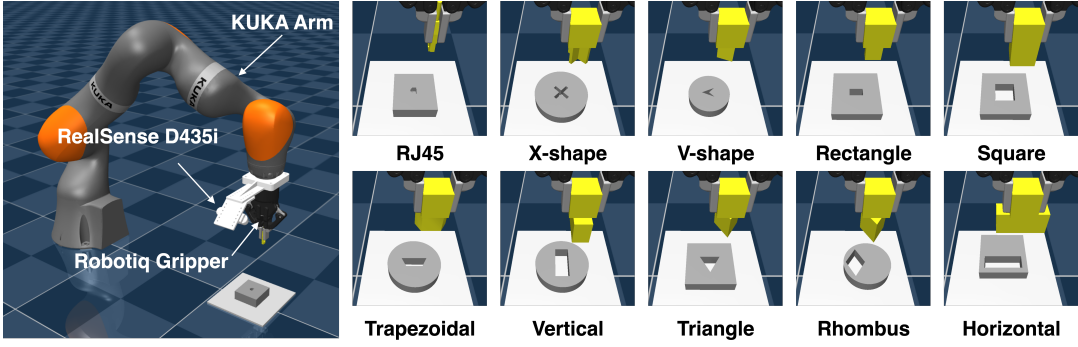


Fig. 3. Simulation setup and peg-in-hole suites with different shapes, where pegs are initialized with being grasped by the gripper

step TD target y is given as

$$y = \sum_{i=0}^{n-1} \gamma^i r_{t+i} + \gamma^n \min_{k=1,2} Q_{\bar{\phi}_k}(\mathbf{h}_{t+n}, \tilde{\mathbf{a}}_{t+n}), \quad (2)$$

where

$$\tilde{\mathbf{a}}_{t+n} = \pi_{\theta}(\cdot | \mathbf{h}_{t+n}) + \epsilon, \quad \epsilon = \text{clip}(\mathcal{N}(0, \sigma^2), -c, c).$$

The weights of the target critic $\bar{\phi}_k$ are updated by Polyak averaging. The policy is learned by minimizing the following loss:

$$\mathcal{L}_{\pi} = \mathbb{E}_{\mathbf{o}_t \sim \mathcal{D}} \left[\min_{k=1,2} Q_{\phi_k}(\mathbf{h}_t, \tilde{\mathbf{a}}_t) \right], \quad \tilde{\mathbf{a}}_t \sim \pi_{\theta}(\cdot | \mathbf{h}_t) + \epsilon. \quad (3)$$

A linear decay schedule or constant can be specified for the standard deviation of the exploration noise according to the task complexity.

B. Separate Primitive Policy

DrQ-v2 is treated as visual RL backbones to exhibit the compatibility of the proposed insertion strategy for the actor-critic framework. Two primitives, location \mathbf{a}_{loc} and insertion \mathbf{a}_{ins} , are designed to control the predefined behaviors of the agent, which are manifested as the output commands on certain dimensions. The actor integrates two policy networks with the same structure to jointly learn the expressions of the above two actions [34], [35]. As shown in Fig. 1, location and insertion run sequentially until success, which means one step of S2P requires two environment steps. Each primitive action is deduced separately based on the corresponding observed state, i.e., $\mathbf{o}_{loc} \rightarrow \mathbf{a}_{loc}$ and $\mathbf{o}_{ins} \rightarrow \mathbf{a}_{ins}$. Thus, POMDP of S2P can be re-defined as $(\mathcal{O}_{loc}, \mathcal{A}_{loc}, \mathcal{P}_{loc}, \mathcal{O}_{ins}, \mathcal{A}_{ins}, \mathcal{P}_{ins}, \mathcal{R}, \gamma)$, where $\mathcal{P}_{loc}(\mathbf{o}_{t+1}^{loc} | \mathbf{o}_t^{loc}, \mathbf{a}_t^{loc})$ and $\mathcal{P}_{ins}(\mathbf{o}_{t+1}^{ins} | \mathbf{o}_t^{ins}, \mathbf{a}_t^{ins})$. The step reward is counted only after the insertion action has been executed, ensuring the feedback specifically reflects the outcome of the insertion operation. The sample batch is composed of $(\mathbf{o}_t^{loc}, \mathbf{a}_t^{loc}, \mathbf{o}_t^{ins}, \mathbf{a}_t^{ins}, r_t)$. An ensemble of four Q -functions is employed to construct the double Q -learning for each state-action pair, i.e., $Q_{\phi_k}(\mathbf{h}_t^{loc}, \mathbf{a}_t^{loc})$ and $Q_{\varphi_k}(\mathbf{h}_t^{ins}, \mathbf{a}_t^{ins}), \forall k = 1, 2$.

The original network architecture of DrQ-v2 is modified to support S2P, which is shown in Fig. 2. Thus, Eqs. 1-3 are

reformulated on the basis of the above statement:

$$y = \sum_{i=0}^{n-1} \gamma^i r_{t+i} + \gamma^n \left(\min_{k=1,2} Q_{\bar{\phi}_k}(\mathbf{h}_{t+n}^{loc}, \tilde{\mathbf{a}}_{t+n}^{loc}) + \min_{k=1,2} Q_{\bar{\varphi}_k}(\mathbf{h}_{t+n}^{ins}, \tilde{\mathbf{a}}_{t+n}^{ins}) \right) \quad (4)$$

$$\mathcal{L}_Q = \mathbb{E}_{\tau \sim \mathcal{D}} \left[\left(Q_{\phi_k}(\mathbf{h}_t^{loc}, \mathbf{a}_t^{loc}) + Q_{\varphi_k}(\mathbf{h}_t^{ins}, \mathbf{a}_t^{ins}) - y \right)^2 \right] \quad (5)$$

$$\mathcal{L}_{\pi} = \mathbb{E}_{\mathbf{o}_t^{loc}, \mathbf{o}_t^{ins} \sim \mathcal{D}} \left[\min_{k=1,2} Q_{\phi_k}(\mathbf{h}_t^{loc}, \tilde{\mathbf{a}}_t^{loc}) + \min_{k=1,2} Q_{\varphi_k}(\mathbf{h}_t^{ins}, \tilde{\mathbf{a}}_t^{ins}) \right], \quad (6)$$

where \mathbf{a}^{loc} and \mathbf{a}^{ins} are sampled from the location π_{θ} and insertion π_{ϑ} policies, respectively. Exploration noise for different actions follows the same linear schedule. However, different noise clip intervals (i.e., ϵ_{loc} and ϵ_{ins}) can be specified to achieve desired explorations:

$$\begin{aligned} \tilde{\mathbf{a}}_t^{loc} &\sim \pi_{\theta}(\cdot | \mathbf{h}_t^{loc}) + \epsilon_{loc} \\ \tilde{\mathbf{a}}_t^{ins} &\sim \pi_{\vartheta}(\cdot | \mathbf{h}_t^{ins}) + \epsilon_{ins}, \end{aligned} \quad (7)$$

where $\epsilon_{loc} \sim \text{clip}(\mathcal{N}(0, \sigma^2), -c_{loc}, c_{loc})$ and $\epsilon_{ins} \sim \text{clip}(\mathcal{N}(0, \sigma^2), -c_{ins}, c_{ins})$. The pseudocode in Algorithm 1 illustrates the interference and training details of S2P-DrQ-v2.

V. EXPERIMENT

A. Setup

All tests in this paper are carried out on the platform shown in Fig. 3, where a connector is utilized to attach the Robotiq 2F-85 gripper to the KUKA LBR IIWA 14 arm and RGB images are obtained from the Realsense D435i wrist camera. The setup in Fig. 3 is intended to match the real-world scenario. Meanwhile, the operational space controller [36] is deployed to enable the compliance contact:

$$\tau = J(q)^T \Lambda(q) (-K_p \Delta x - K_d \dot{x}) + C(q, \dot{q}) + G(q), \quad (8)$$

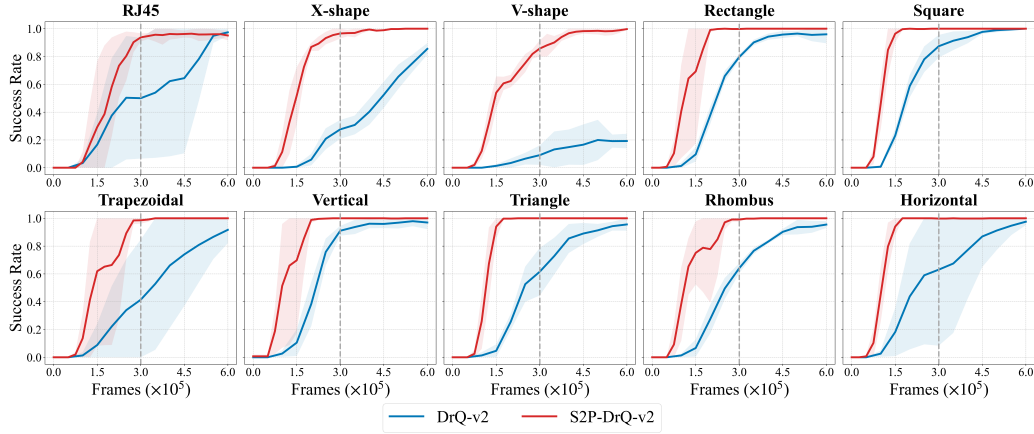


Fig. 4. Training performance of S2P against the plain policy, where the solid line and the shaded area represent the mean and standard deviation across 3 runs.

Algorithm 1 Training details for S2P-DrQ-v2

Require: Actors $\pi_\theta, \pi_\vartheta$, critics $Q_{\phi_k}, Q_{\varphi_k}$, visual encoder f_ξ , learning rate η , replay buffer \mathcal{D} , training frames T , exploration noise schedule σ_t , standard deviation clip intervals c_{loc}, c_{ins} , batch size, Polyak average rate μ , and UTD ratio

```

1: for  $t = 1 \dots T$  do
2:    $\mathbf{a}_t^{loc} \leftarrow \pi_\theta \left( \cdot | f_\xi \left( \text{aug} \left( \mathbf{o}_t^{loc} \right) \right) \right)$ 
3:    $\mathbf{o}_{t+1}^{loc} \leftarrow \mathcal{P} \left( \cdot | \mathbf{o}_t^{loc}, \mathbf{a}_t^{loc} \right)$ 
4:    $\mathbf{a}_t^{ins} \leftarrow \pi_\vartheta \left( \cdot | f_\xi \left( \text{aug} \left( \mathbf{o}_t^{ins} \right) \right) \right)$ 
5:    $\mathbf{o}_{t+1}^{ins} \leftarrow \mathcal{P} \left( \cdot | \mathbf{o}_t^{ins}, \mathbf{a}_t^{ins} \right)$ 
6:    $\mathcal{D} \leftarrow \mathcal{D} \cup \left( \mathbf{o}_t^{loc}, \mathbf{o}_t^{ins}, \mathbf{a}_t^{loc}, \mathbf{a}_t^{ins}, r_t, \mathbf{o}_{t+1}^{loc}, \mathbf{o}_{t+1}^{ins} \right)$ 
7:    $\mathcal{B} \leftarrow \mathcal{D}$  ▷ Sample batch transitions
8:   for  $j = 1 \dots \text{UTD}$  do
9:     UPDATECRITIC( $\mathcal{B}, \sigma_t$ ) with Eq. 5
10:    UPDATEACTOR( $\mathcal{B}, \sigma_t$ ) with Eq. 6
11:   end for
12: end for

```

where $\tau \in \mathbb{R}^7$ is the joint torque vector. $J(q) \in \mathbb{R}^{6 \times 7}$ is the task Jacobian matrix. $\Lambda(q) = \left(J(q) M(q)^{-1} J(q)^T \right)^{-1}$ is the operational space inertial matrix. $M(q) \in \mathbb{R}^{7 \times 7}$ is the joint-space inertia matrix. $K_p, K_d \in \mathbb{R}^7$ are diagonal elements of PD gains. $x, \dot{x} \in \mathbb{R}^6$ are twist and velocity vectors of the end-effector in the task space. $C(q, \dot{q})$ is the Coriolis and Centrifugal forces, and $G(q)$ is the gravity vector. The KUKA arm is empowered with 4 feasible degrees of freedom, i.e., translation along the x, y, and z axes in Cartesian space and rotation around the yaw axis. Each training episode is reset with a randomized end-effector pose within $\pm[0.02, 0.02, 0.03]$ m and ± 0.3 rad intervals. We integrate a suite of peg-in-hole tasks containing different types of pegs and holes, which are shown in Fig. 3. Each task is initialized with the peg already grasped by the gripper. This suite, powered by MuJoCo, contains different pegs and holes with basic polygons and extra challenging shapes. RJ45, X-shape, and V-shape are freshly designed, and the rest are

inherited from the open-sourced assets¹.

B. Evaluations

Training Details. Three consecutive frames with 96×96 size are adopted as observations that are passed to the visual encoder to obtain the low-dimensional representation. 60K training frames are assigned to all tasks. Success rate is utilized as the evaluation metric to observe the sample efficiency and performance. A staged dense reward that applies to all tasks is designed to facilitate convergence:

$$r_t = \max \begin{cases} w_r (1 - \tanh(\lambda \cdot \Delta s_1)) & \text{(reaching)} \\ 3 + w_a (1 - \Delta s / \varepsilon_a) & \text{if } \Delta s_1 \leq \varepsilon_a \ \& \ \Delta \delta \leq \delta_a \text{ (alignment)} \\ 4 + w_i h & \text{if } h \leq 0 \ \& \ \text{alignment achieved (insertion)} \\ 10 & \text{if } \Delta s_2 \leq \varepsilon_f \text{ (completion),} \end{cases} \quad (9)$$

where w_r , w_a , and w_i are reward weights for different stages. The relative distances from the peg tip to the surface and bottom of the hole are indicated as Δs_1 and Δs_2 , respectively. $\Delta \delta$ is the orientation error. ε_a , δ_a , and ε_f are pose thresholds at different stages. h is the insertion depth. Once the completion signal is detected, the current episode will be marked as successful and then truncated. The whole training process is accomplished with an NVIDIA 4080 GPU and an i7-12700K CPU. The comparison results are obtained using the following methods:

- S2P-DrQ-v2: S2P is built on DrQ-v2. Two separate policy networks are integrated in the actor, which deduces the location $\mathbf{a}_{loc} \in \mathbb{R}^4$ and insertion $\mathbf{a}_{ins} \in \mathbb{R}$ actions, respectively. \mathbf{a}_{ins} only denotes the vertical motion along the z-axis of Cartesian space.
- DrQ-v2: A plain policy built on DrQ-v2 derives $\mathbf{a} \in \mathbb{R}^4$.

As described in Section IV, one step of S2P consumes two environment steps. An action repeat (AR) of 2 is assigned

¹https://github.com/carlosferrazza/tactile_envs.
git

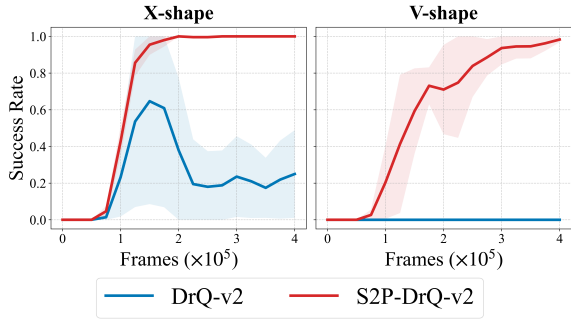


Fig. 5. Benchmark results of S2P-DrQ-v2 and DrQ-v2 with force penalty.

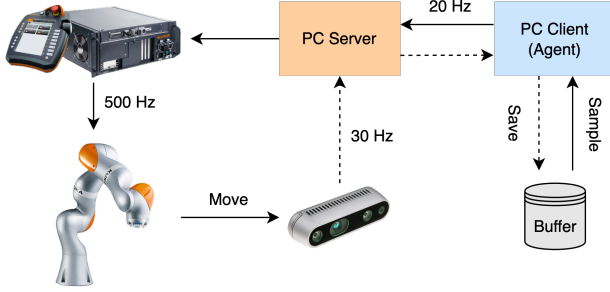


Fig. 6. Training procedure and communication network on the real platform.

to the plain policy to align the consistent maximum episode length with S2P. All the above methods are trained on the premise of $UTD = 2$ to improve the underlying sample efficiency. The hyperparameters used for training are given in Appendix.

Evaluation Results. Fig. 4 presents the training results for ten tasks, where each policy is evaluated through 3 different seeds. S2P-DrQ-v2 outperforms the plain policy in terms of sampling efficiency, which benefits from additional insertion action \mathbf{a}_{ins} to reach the hole surface faster. Meanwhile, the exploration of location policy can be narrowed through \mathbf{a}_{ins} to output deterministic location actions. \mathbf{a}_{ins} is scheduled in advance as a chain of sequential actions to increase the number of insertion attempts. Although AR can be used to enable similar exploration and reinforce perception of the current action, we found this is less effective than establishing a policy to independently learn the insertion action. As shown in Fig. 4, for the challenging V- and X-shape tasks, S2P is able to substantially improve the success rate while enhancing the sample efficiency. The gray dashed lines in Fig. 4 indicate the success rates of different methods in the middle of the training period to quantify the performance comparison. For most tasks, S2P-DrQ-v2 achieves a performance gain of 20%-30% relative to the plain policy, especially for the case with complex polygons. Notably, S2P attains a $\sim 100\%$ success rate with only half of the training frames.

Furthermore, S2P can unleash its power when facing more severe constraints. The force penalty is added to Eq. 9 to more accurately reflect the real-world scenarios. A force

threshold of 15 N is given to penalize the brute insertion action, i.e., $r_f = w_f \cdot \|f_{ee} - f_{max}\|_2$. System identification is first executed in the simulation environment to estimate the end-effector load and thus obtain accurate external force data from the sensor. Only representative X- and V- shape tasks are adopted for comparison to save computational resources. The location policy of S2P derives an action of $\mathbf{a}_{loc} \in \mathbb{R}^3$ without movement along the z-axis in Cartesian space, allowing the insertion policy of S2P to specialize in learning compliant insertion behavior. Meanwhile, the action sequence of DrQ-v2 is planned as $\mathbf{a}_0 = (a_x, a_y, 0, a_r) \rightarrow \mathbf{a}_1 = (0, 0, a_z, 0)$ to mimic the locate-then-insert behavior of S2P. Fig. 5 indicates that DrQ-v2 fails to complete the aforementioned tasks. The entire training process of DrQ-v2 is unstable and non-convergent. Despite additional force constraints, S2P achieves remarkable sample efficiency success rates, rivaling the benchmark results in Fig. 4. These comparison results further demonstrate that learning the insertion primitive via a separate policy enables more flexible adaptation to diverse scenarios.

C. Real-World Experiments

The feasibility of S2P is verified in this section on the real platform. The KUKA controller, RealSense D435i, PC client, and server are the major components of the communication network, which can be observed in Fig. 6. The PC client integrates the training framework and transmits the actor command to the PC server, which constructs the communication bridge between the KUKA controller and the PC client. All data transmission is implemented through socket connections. The Cartesian impedance mode is predefined in the controller and executed in the background. As shown in Fig. 7, the setup of the experimental platform is basically consistent with that of the simulation. Due to the high training cost on the real platform, only the X-shape task is considered in this section. The wall-clock time for training in the real world is about 4 hours. Fig. 7 also illustrates one of the completed insertion processes via the trained S2P-DrQ-v2 model, which attains a success rate of 20/20.

D. Ablations

This section performs some ablation experiments to discuss the hyperparameters of S2P-DrQ-v2 that could impact the performance and the generalization for other off-policy algorithms like Soft Actor-Critic. Similarly, for computational resources, the following ablation experiments are restricted to force-penalized X- and V-shape tasks.

Action repeat. AR is a widely used technique to enhance the recognition of actions that trigger high rewards and thus accelerate the sample efficiency. The location and insertion actions of S2P require two consecutive environment steps, which exhibit identical temporal characteristics to $AR = 2$ for the plain policy. Therefore, all evaluations on S2P in previous sections are performed without AR. This part will explore whether AR will further improve the sample efficiency and success rate. As shown in Fig. 8, $AR = 2$ fails to improve the performance of S2P and decreases the

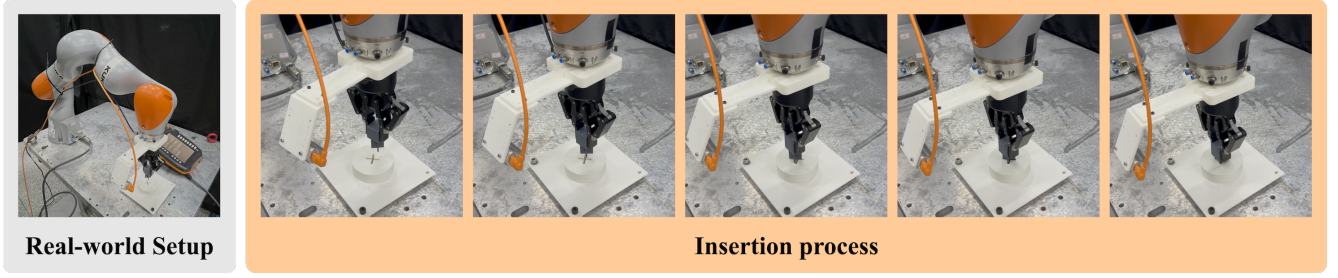


Fig. 7. Real-world platform setup and a completed insertion process with the trained model of S2P-DrQ-v2.

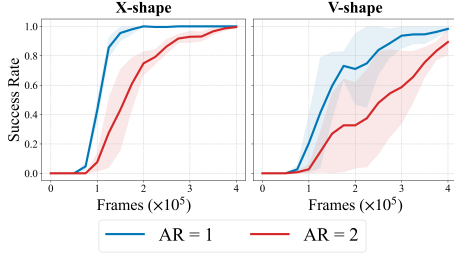


Fig. 8. Ablation analysis on the effect of action repeat on S2P-DrQ-v2.

sample efficiency. Especially for the V-shape task, $AR = 2$ oscillates training processes with wider standard deviation intervals. Unlike the plain policy, S2P specializes in separate adjustments of location and insertion actions based on corresponding observations, which enables a flexible response to frequent changes in contact states and thus refines primitive actions. Such a property of S2P is efficient when there exist force constraints. However, action repeat extends the reaction period to two steps, which adversely slows the learning process.

Generalize to Soft Actor-Critic. S2P is adapted to the actor-critic framework. Thus, we extend S2P to the Soft Actor-Critic (i.e., S2P-SAC) to investigate whether similar performance gains can be achieved, despite prior research [26] demonstrating the poor performance of SAC in visual continuous control tasks. The implementation details of S2P-SAC can be summarized as follows:

$$y = \sum_{i=0}^{n-1} \gamma^i r_{t+i} + \gamma^n \left(\left(\min_{k=1,2} Q_{\bar{\phi}_k}(\mathbf{h}_{t+n}^{loc}, \tilde{\mathbf{a}}_{t+n}^{loc}) - \alpha_{loc} \log \pi_{\theta}(\tilde{\mathbf{a}}_{t+n}^{loc} | \mathbf{h}_{t+n}^{ins}) \right) + \left(\min_{k=1,2} Q_{\bar{\phi}_k}(\mathbf{h}_{t+n}^{ins}, \tilde{\mathbf{a}}_{t+n}^{ins}) - \alpha_{ins} \log \pi_{\vartheta}(\tilde{\mathbf{a}}_{t+n}^{ins} | \mathbf{h}_{t+n}^{ins}) \right) \right) \quad (10)$$

$$\mathcal{L}_{\pi} = \mathbb{E}_{\mathbf{o}_t \sim \mathcal{D}} \left[\left(\min_{k=1,2} Q_{\phi_k}(\mathbf{h}_t^{loc}, \tilde{\mathbf{a}}_t^{loc}) - \alpha_{loc} \log \pi_{\theta}(\tilde{\mathbf{a}}_t^{loc} | \mathbf{h}_t^{loc}) \right) + \left(\min_{k=1,2} Q_{\varphi_k}(\mathbf{h}_t^{ins}, \tilde{\mathbf{a}}_t^{ins}) - \alpha_{ins} \log \pi_{\vartheta}(\tilde{\mathbf{a}}_t^{ins} | \mathbf{h}_t^{ins}) \right) \right] \quad (11)$$

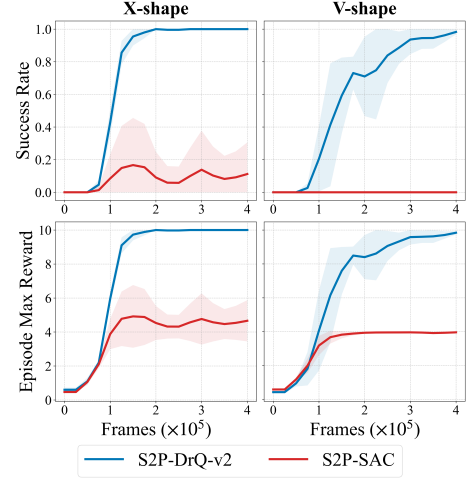


Fig. 9. Ablation study on extending S2P to SAC, where the success rate and maximum episode reward are statistically averaged based on all completed episodes within each log cycle.

$$\mathcal{L}_{\alpha} = \mathbb{E}_{\tilde{\mathbf{a}}_t^{loc} \sim \pi_{\theta}, \tilde{\mathbf{a}}_t^{ins} \sim \pi_{\vartheta}} \left[-\alpha_{loc} \log \pi_{\theta}(\tilde{\mathbf{a}}_t^{loc} | \mathbf{h}_t^{loc}) - \alpha_{loc} \mathcal{H}(\pi_{\theta}(\tilde{\mathbf{a}}_t^{loc} | \mathbf{h}_t^{loc})) - \alpha_{ins} \log \pi_{\vartheta}(\tilde{\mathbf{a}}_t^{ins} | \mathbf{h}_t^{ins}) - \alpha_{ins} \mathcal{H}(\pi_{\vartheta}(\tilde{\mathbf{a}}_t^{ins} | \mathbf{h}_t^{ins})) \right], \quad (12)$$

where α_{loc} and α_{ins} are temperature coefficients for entropy regularization of corresponding policies. \mathcal{H} is the entropy term. The critic loss of S2P-SAC can also be obtained via Eq. 5. Fig. 9 illustrates the training process of S2P-SAC on challenging tasks, where S2P is not able to enhance the exploration of SAC to find the optimal full insertion state with the force penalty. We observe the maximum episode reward from the second row of Fig. 9 and find that S2P-SAC can only search for suboptimal states above the hole upper surface. These ablation results further show that S2P can enhance the performance of visual RL algorithms under severe constraints but cannot compensate for the deficiencies of visual RL algorithms on exploration.

VI. CONCLUSION

This paper presents S2P based on visual reinforcement learning. S2P utilizes an ensemble of actors and critics to learn location and insertion actions, which are executed sequentially and can be generalized to one action response to

the environment. S2P shows superior sample efficiency and success rates across different insertion tasks and can even explore the optimal state with force penalty. Physical experiments are performed to further validate the feasibility of S2P. Ablation study indicates that S2P fails to perform well on SAC compared to DrQ-v2. Future work will optimize the primitive strategy to alleviate the dependence on underlying visual RL algorithms.

APPENDIX

Generalized and specified hyperparameters used for training all the tasks above will be listed in this section.

TABLE I

HYPERPARAMETERS USED FOR TRAINING DRQ-V2 AND S2P-DRQ-V2

Hyperparameters	Value
Image size	$96 \times 96 \times 3$
Image augmentation	RandomShift (pad=4)
Frame stack	3
Discount factor γ	0.99
Replay Buffer size	$1e7$
Batch size	256
N-step return	3
Optimizer	Adam
Learning Rate	$1e-4$
UTD ratio	2
Max episode steps	200
Linear decaying schedule	linear (1.0, 0.1, 30000)
Action repeat	1 (S2P-DrQ-v2) / 2 (DrQ-v2)
CNN architecture	Conv (c=[32, 64, 128, 256], s=2, p=1)
MLP architecture	Linear (c=[64, 1024, 1024], bias=True)
w_r, w_a	1, 2
w_i	70 (RJ45) / 40 (Others)
$\lambda, \varepsilon_a, \delta_a, \varepsilon_f$	10, 5 mm, 0.05 rad, 1 mm

TABLE II

SPECIALIZED HYPERPARAMETERS USED FOR TRAINING TASKS IN FIG. 5

Hyperparameters	Value
Force penalty weight	-0.8 (X-shape) / -0.5 (V-shape)
Force penalty threshold	15 N
Noise clip intervals	$\varepsilon_{loc}, \varepsilon_{ins} = 0.3$ (S2P-DrQ-v2) / 0.3 (DrQ-v2)
Action repeat	1

REFERENCES

- [1] Z. Yuan, Z. Xue, B. Yuan, X. Wang, Y. Wu, Y. Gao, and H. Xu, "Pre-Trained Image Encoder for Generalizable Visual Reinforcement Learning," in *Conference on Neural Information Processing Systems (NeurIPS)*, 2022.
- [2] G. Lee, J. Lee, S. Noh, M. Ko, K. Kim, and K. Lee, "Polyfit: A Peg-in-hole Assembly Framework for Unseen Polygon Shapes via Sim-to-real Adaptation," in *IEEE/RJS International Conference on Intelligent Robots and Systems (IROS)*, vol. abs/2312.02531, 2024, pp. 533–540.
- [3] C. Sferazza, Y. Seo, H. Liu, Y. Lee, and P. Abbeel, "The Power of the Senses: Generalizable Manipulation from Vision and Touch through Masked Multimodal Learning," in *IEEE/RJS International Conference on Intelligent Robots and Systems (IROS)*, vol. abs/2311.00924, 2024, pp. 9698–9705.
- [4] N. Hansen, Z. Yuan, Y. Ze, T. Mu, A. Rajeswaran, H. Su, H. Xu, and X. Wang, "On Pre-Training for Visuo-Motor Control: Revisiting a Learning-from-Scratch Baseline," in *International Conference on Machine Learning (ICML)*, 2023, pp. 12 511–12 526.
- [5] Z. Yuan, T. Wei, S. Cheng, G. Zhang, Y. Chen, and H. Xu, "Learning to Manipulate Anywhere: A Visual Generalizable Framework For Reinforcement Learning," in *8th Annual Conference on Robot Learning*, 2024.
- [6] N. Hansen, H. Su, and X. Wang, "Stabilizing Deep Q-Learning with ConvNets and Vision Transformers under Data Augmentation," in *Conference on Neural Information Processing Systems (NeurIPS)*, 2021, pp. 3680–3693.
- [7] S. Nasiriany, H. Liu, and Y. Zhu, "Augmenting Reinforcement Learning with Behavior Primitives for Diverse Manipulation Tasks," in *2022 International Conference on Robotics and Automation (ICRA)*. IEEE, 2022, pp. 7477–7484.
- [8] N. Vuong, H. Pham, and Q.-C. Pham, "Learning Sequences of Manipulation Primitives for Robotic Assembly," in *2021 IEEE International Conference on Robotics and Automation (ICRA)*. IEEE, 2021.
- [9] X. Chen, C. Wang, Z. Zhou, and K. W. Ross, "Randomized Ensembled Double Q-Learning: Learning Fast Without a Model," in *International Conference on Learning Representations (ICLR)*, 2021.
- [10] G. Ma, L. Li, S. Zhang, Z. Liu, Z. Wang, Y. Chen, L. Shen, X. Wang, and D. Tao, "Revisiting Plasticity in Visual Reinforcement Learning: Data, Modules and Training Stages," in *International Conference on Learning Representations (ICLR)*, 2024.
- [11] S. Kozlovsky, E. Newman, and M. Zacksenhouse, "Reinforcement Learning of Impedance Policies for Peg-in-Hole Tasks: Role of Asymmetric Matrices," *IEEE Robotics and Automation Letters*, vol. 7, no. 4, pp. 10 898–10 905, 2022.
- [12] Kimble, Kenneth, Van, Wyk, Karl, Falco, Joe, Messina, Elena, Sun, Yu, Shibata, Mizuho, Uemura, Wataru, Yokokohji, and Yasuyoshi, "Benchmarking Protocols for Evaluating Small Parts Robotic Assembly Systems," *IEEE Robotics and Automation Letters*, 2020.
- [13] W. Chen, C. Zeng, H. Liang, F. Sun, and J. Zhang, "Multimodality Driven Impedance-Based Sim2Real Transfer Learning for Robotic Multiple Peg-in-Hole Assembly," *IEEE Transactions on Cybernetics*, pp. 1–14, 2024.
- [14] P. Jin, B. Huang, W. W. Lee, T. Li, and W. Yang, "Visual-Force-Tactile Fusion for Gentle Intricate Insertion Tasks," *IEEE Robotics and Automation Letters*, pp. 1–8, 2024.
- [15] S. Dong, D. K. Jha, D. Romeres, S. Kim, D. Nikovski, and A. Rodriguez, "Tactile-RL for Insertion: Generalization to Objects of Unknown Geometry," in *2021 IEEE International Conference on Robotics and Automation (ICRA)*. IEEE, 2021, pp. 6437–6443.
- [16] J. Luo, E. Solowjow, C. Wen, J. A. Ojeda, A. M. Agogino, A. Tamar, and P. Abbeel, "Reinforcement Learning on Variable Impedance Controller for High-Precision Robotic Assembly," in *2019 International Conference on Robotics and Automation (ICRA)*. IEEE, 2019, pp. 3080–3087.
- [17] I. Akinola, J. Xu, J. Carius, D. Fox, and Y. S. Narang, "Tacsl: A Library for Visuotactile Sensor Simulation and Learning," *IEEE Transactions on robotics*, vol. abs/2408.06506, 2024.
- [18] A. Y. Yasutomi, H. Ichiwara, H. Ito, H. Mori, and T. Ogata, "Visual Spatial Attention and Proprioceptive Data-Driven Reinforcement Learning for Robust Peg-in-Hole Task Under Variable Conditions," *IEEE Robotics and Automation Letters*, vol. 8, no. 3, pp. 1834–1841, 2023.
- [19] Y. Shi, Z. Chen, H. Liu, S. Riedel, C. Gao, Q. Feng, J. Deng, and J. Zhang, "Proactive Action Visual Residual Reinforcement Learning for Contact-Rich Tasks Using a Torque-Controlled Robot," in *IEEE International Conference on Robotics and Automation (ICRA)*, 2021, pp. 765–771.
- [20] B. Tang, I. Akinola, J. Xu, B. Wen, A. Handa, K. V. Wyk, D. Fox, G. S. Sukhatme, F. Ramos, and Y. S. Narang, "Automate: Specialist and Generalist Assembly Policies over Diverse Geometries," in *Robotics: Science and Systems Conference (RSS)*, 2024.
- [21] X. Zhang, S. Jin, C. Wang, X. Zhu, and M. Tomizuka, "Learning Insertion Primitives with Discrete-Continuous Hybrid Action Space for Robotic Assembly Tasks," in *2022 International Conference on Robotics and Automation (ICRA)*. IEEE, 2022, pp. 9881–9887.
- [22] Y. Ze, Y. Liu, R. Shi, J. Qin, Z. Yuan, J. Wang, and H. Xu, "H-InDex: Visual Reinforcement Learning with Hand-Informed Representations for Dexterous Manipulation," in *Conference on Neural Information Processing Systems (NeurIPS)*, 2023.
- [23] D. Bertoin, A. Zouitine, M. Zouitine, and E. Rachelson, "Look where you look! Saliency-guided Q-networks for generalization in visual Reinforcement Learning," in *Conference on Neural Information Processing Systems (NeurIPS)*, 2022.

- [24] M. Laskin, K. Lee, A. Stooke, L. Pinto, P. Abbeel, and A. Srinivas, "Reinforcement Learning with Augmented Data." in *Conference on Neural Information Processing Systems (NeurIPS)*, 2020.
- [25] D. Yarats, I. Kostrikov, and R. Fergus, "Image Augmentation Is All You Need: Regularizing Deep Reinforcement Learning from Pixels." in *International Conference on Learning Representations (ICLR)*, 2021.
- [26] D. Yarats, R. Fergus, A. Lazaric, and L. Pinto, "Mastering Visual Continuous Control: Improved Data-Augmented Reinforcement Learning." in *International Conference on Learning Representations (ICLR)*, 2022.
- [27] A. Almuzairee, N. Hansen, and H. I. Christensen, "A Recipe for Unbounded Data Augmentation in Visual Reinforcement Learning." *Reinforcement Learning Conference (RLC)*, vol. 1, pp. 130–157, 2024.
- [28] R. Zheng, X. Wang, Y. Sun, S. Ma, J. Zhao, H. Xu, H. D. III, and F. Huang, "Taco: Temporal Latent Action-Driven Contrastive Loss for Visual Reinforcement Learning." in *Conference on Neural Information Processing Systems (NeurIPS)*, 2023.
- [29] S. Nair, A. Rajeswaran, V. Kumar, C. Finn, and A. Gupta, "R3m: A Universal Visual Representation for Robot Manipulation." in *Conference on Robot Learning (CoRL)*, 2022, pp. 892–909.
- [30] G. Jiang, Y. Sun, T. Huang, H. Li, Y. Liang, and H. Xu, "Robots Pre-train Robots: Manipulation-Centric Robotic Representation from Large-Scale Robot Dataset," in *The Thirteenth International Conference on Learning Representations*, vol. abs/2410.22325, 2025.
- [31] R. Bellman, "A markovian decision process." *Journal of mathematics and mechanics*, pp. 679–684, 1957.
- [32] T. P. Lillicrap, J. J. Hunt, A. Pritzel, N. Heess, T. Erez, Y. Tassa, D. Silver, and D. Wierstra, "Continuous control with deep reinforcement learning," *arXiv*, 2015.
- [33] S. Fujimoto, H. Hoof, and D. Meger, "Addressing function approximation error in actor-critic methods," in *International conference on machine learning*. PMLR, 2018, pp. 1587–1596.
- [34] W. Huang, I. Mordatch, and D. Pathak, "One policy to control them all: Shared modular policies for agent-agnostic control," in *International Conference on Machine Learning*. PMLR, 2020, pp. 4455–4464.
- [35] J. Shang and M. S. Ryoo, "Active Vision Reinforcement Learning under Limited Visual Observability." in *Conference on Neural Information Processing Systems (NeurIPS)*. arXiv, 2023.
- [36] O. Khatib, "A unified approach for motion and force control of robot manipulators: The operational space formulation." *IEEE Transactions on Robotics*, vol. 3, no. 1, pp. 43–53, 1987.